



1 Quantifying changes in seasonal temperature variations using a 2 functional data analysis approach

3 Eva Holtanová¹, Jan Koláček², Lukas Brunner³

4 ¹Department of Atmospheric Physics, Faculty of Mathematics and Physics, Charles University, V Holešovičkách 2, Prague,
5 180 00, Czech Republic

6 ²Department of Mathematics and Statistics, Faculty of Science, Masaryk University, Kotlářská 267/2, 611 37, Brno, Czech
7 Republic

8 ³Research Unit Sustainability and Climate Risk, Center for Earth System Research and Sustainability (CEN), University of
9 Hamburg, Hamburg, Germany

10

11

12 *Correspondence to:* Eva Holtanová (eva.holtanova@matfyz.cuni.cz), Lukas Brunner (lukas.brunner@uni-hamburg.de)

13 **Abstract.** Ever-worsening climate change increases near-surface air temperatures for almost the entire Earth and threatens
14 living organisms and human society. While annual mean changes are frequently used to quantify past and expected future
15 changes, the increase is rarely uniform throughout the year. In addition, the shape of the annual cycle and its changes can differ
16 considerably between regions around the globe. Therefore, we perform a global analysis resolving the annual cycle and its
17 changes in different regions, focusing on diagnostics that can be evaluated for various existing annual cycle shapes (e.g., single
18 and double waves, different timing of seasons, etc.). Many previous studies relied on parameter-based methods, assuming a
19 sinusoidal shape of the mean annual cycle. Here, we introduce an innovative approach based on Functional Data Analysis
20 (FDA), a relatively new statistical approach. The evolution of the mean annual cycle is estimated from daily long-term mean
21 temperature values, which are converted to functional form. We concentrate on diagnostics that evaluate the change in absolute
22 temperature, its seasonal slope, the position of the maximum, and the amplitude of the annual cycle. We analyze two reanalysis
23 datasets (coupled CERA20C and atmospheric ERA5) and a subset of five CMIP6 Earth system models (ESMs). Observed
24 changes in the second half of the 20th century are assessed, and the ability of ESMs to represent them is evaluated. Further,
25 the changes projected for the end of the 21st century under the SSP3-7.0 pathway are analyzed. Among other results, we
26 highlight distinct differences between the two reanalyses, especially over equatorial and polar regions across diagnostics. Our
27 approach also reveals that differences in the historical period between 1951-1980 and 1981-2010 can be negative during (short)
28 parts of the year in many regions. Further, the ESMs future projections show different rates of warming between seasons,
29 resulting in changes in the amplitude. The largest amplitude increase is projected over the Mediterranean region, and the largest
30 decrease over the Arctic Ocean, the latter being due to the considerably stronger warming in the northern hemisphere winter.
31 The ESMs also project a delayed maximum near the poles and an earlier maximum in many tropical continental regions. In



32 Europe, the southern and eastern regions experienced a delay of the maximum of up to 10 days, whereas a slightly earlier
33 maximum is found for northern Europe. A similar dipole pattern can be seen between eastern and western regions in North
34 America. Regarding the slope of the annual cycle, higher latitudes detect a higher magnitude of change in the historical period
35 than lower latitudes. The geographical pattern remains the same for future slope changes, with the magnitude twice as high in
36 most regions. The FDA diagnostics introduced here can be tailored for different purposes and applied to other climatic
37 variables, without making any prior assumptions about the annual cycle shape. Potential applications include, e.g., explicitly
38 evaluating the climate model performance or ensemble mean and spread assessment beyond annual or seasonal means.

39 **1 Introduction**

40 Increasing near-surface air temperature is observed and projected for almost the entire Earth (IPCC, 2021), threatening the
41 environment and human society alike. However, this temperature increase is rarely uniform throughout the year, and even if
42 the annual mean changes only slightly, the annual cycle might change quite dramatically (Marvel et al., 2021; Wang et al.,
43 2021). The changes in seasonal temperature cycle can have potentially large impacts on, e.g., phenological phases of living
44 organisms, agriculture, health, tourism, and other sectors. Widespread expected changes in the annual cycle have even
45 motivated suggestions of new definitions of seasons (Wang et al., 2021; López-Franca et al., 2022). Moreover, as noted by
46 McKinon and Huybers (2024), the shape of the temperature annual cycle can be taken as an analogy for temperature changes
47 in general, as it is easily distinguishable from internal variability and can be reliably observed. They emphasize that the
48 seasonality of temperature in the current climate and its changes are strongly related to projected temperature changes, and
49 recent changes in the mean annual cycle can be considered a proxy for overall future warming. The skill of climate models in
50 depicting correctly the observed shape of the annual cycle and its changes is therefore very informative in terms of confidence
51 in simulated future changes (Lynch et al., 2016).

52 A large number of previous studies have shown that the shape of the temperature annual cycle has already changed in recent
53 decades, including, e.g., a phase shift towards an earlier onset of the seasons over the middle and higher latitudes (evaluated
54 using the sinusoidal approximation of the mean annual cycle shape, the results do not relate to a specific season, Stine et al.,
55 2009), lengthening of summer (Park et al., 2018) and shortening of all other seasons over Northern Hemisphere midlatitudes
56 (Wang et al., 2021). Wang and Dillon (2014) revealed regionally different changes of annual cycle amplitude over northern
57 hemisphere midlatitudes and polar regions, with a prevailing decrease in 1975-2010 in comparison to 1961-1990. In addition
58 to adaptation to recently observed shifts, it is also crucial to investigate the expected future evolution, as the shape of the annual
59 cycle is expected to undergo even more dramatic changes during the upcoming decades. For example, Santer et al. (2018,
60 2022) found an increase in the temperature amplitude globally and throughout the troposphere in recent observations and future
61 projections and attributed it to anthropogenic forcing. Further, Chen et al. (2019) concluded that the CMIP5 global climate
62 models project increased seasonal amplitudes in low-latitude regions and most global ocean areas. In contrast, the seasonal
63 amplitudes are expected to decrease over the Southern Ocean and high-latitude regions.



64 Earth system models (ESMs) are state-of-the-art instruments for assessing possible future climate evolutions and attributing
65 observed and projected climate changes to their potential causes. The multi-model ensemble produced under the Coupled
66 Model Intercomparison Project Phase 6 (CMIP6) initiative, coordinated by the World Climate Research Programme's (WCRP)
67 Working Group on Coupled Modelling (Eyring et al., 2016), represents the newest set of ESM simulations. This ensemble
68 includes simulations of a range of different models under several shared socioeconomic pathways (SSPs, Tebaldi et al., 2021),
69 enabling the analysis of uncertainties arising from structural model differences (Abramowitz et al., 2019). Indeed, despite
70 indisputable progress in the complexity of the newest generation ESMs, many uncertainties and issues still need to be solved
71 (Shaw and Stevens, 2025; Randall et al., 2019; Bordoni et al., 2024). The problem of the choice of ESMs appropriate for
72 climate change scenarios is a very complex task, and different approaches are still under investigation (e.g., McDonnel et al.,
73 2024; Snyder et al., 2024; Merrifield et al., 2023; Rahimpour Asenjan et al., 2023).

74 The shape of the annual cycle of air temperature differs significantly among different regions around the globe. Therefore, a
75 global analysis requires focusing on quantities that can be evaluated for all these different shapes (e.g., single and double
76 waves, different timing of seasons, etc.). A lot of previous studies relied on Fourier-transform-based methods, assuming a
77 sinusoidal shape of the mean annual cycle and focused on its amplitude and phase (e.g., in Paluš et al., 2005, Stine et al., 2009,
78 Zhao et al., 2021, Marvel et al., 2021, Deng and Fu, 2023, Zhang et al., 2025), which in some cases resulted in omitting certain
79 regions (e.g., Dwyer et al., 2012, Yettella and England, 2018) and a large portion of studies focused on the northern hemisphere
80 only. Here, we introduce an innovative approach based on Functional Data Analysis (FDA). The evolution of temperature
81 throughout the year is approximated by daily long-term mean temperature values, which are converted to functional form (see
82 Section 3 for details). This approach allows us to assess any existing shape of the temperature seasonal cycle. López-Franca
83 et al. (2022) also employed smoothing of daily temperature values with splines and evaluated changes in dates of minimum
84 and maximum of the smoothed annual cycle and the dates of minimum and maximum slope changes. Unlike the methodology
85 presented here, they only concentrated on specific parts of the year and the midlatitude regions. We previously successfully
86 applied a Functional data analysis approach to investigate the influence of driving the global climate model on nested regional
87 climate simulation within a multi-model ensemble (Holtanová et al., 2019).

88 **2 Data**

89 The present study deals with the mean annual cycle of near-surface air temperature. To analyze its recent changes over both
90 land and ocean regions, we use two reanalysis datasets from the European Centre for Medium-Range Weather Forecasts
91 (ECMWF), namely the ERA5 (Hersbach et al., 2020) and CERA20C (Laloyaux et al., 2018). The choice was motivated by
92 the long temporal coverage of these datasets back to the 1950s. Some basic information about these datasets is described in
93 Table 1. One of the main differences between them is that ERA5 is an atmospheric reanalysis; in contrast, CERA20C was
94 created using a coupled modeling system with the representation of not only the atmosphere but also the ocean, land, oceanic
95 waves, and sea ice. The atmospheric modeling system (ECMWF's Integrated Forecast System (IFS) version CY41R2) is the



96 same for both ERA5 and CERA20C (Laloyaux et al., 2018; Hersbach et al., 2020). As the coupling demands large
97 computational costs, CERA20C has a coarser horizontal resolution (Tab. 1). The CERA20C dataset includes 10 members
98 representing the spread related to the errors in the assimilated observations and the modeling system (Laloyaux et al., 2018).
99 We use the “number0” ensemble member and do not analyze the uncertainty spread here.

100 Further, we select historical and scenario simulations of five CMIP6 ESMs (Table 2). The model choice is motivated by the
101 different values of the equilibrium climate sensitivity (Meehl et al., 2020) and overall good performance compared to the whole
102 CMIP6 ensemble (Bock et al., 2020). We employ only five models to be able to analyze the individual simulated curves of the
103 mean annual cycle and illustrate the innovative methodology properly. For the scenario period, we analyze outputs for the
104 SSP3-7.0 socio-economic pathway, representing the medium to high end of the whole range of the SSPs currently considered
105 plausible (Tebaldi et al., 2021).

106 The analysis focuses on the periods described in Table 3. The two historical periods are used to assess recent observed changes
107 (Section 4.1). The difference between the future and reference periods is the projected or expected future change (described in
108 Section 4.2). For both the reanalyses and ESMs, the long-term mean values of near-surface air temperature for each day of the
109 year are averaged over the reference regions from Working Group 1 of the IPCC AR6 (Iturbide et al. 2020) directly from the
110 native grids. These daily long-term mean values are then subject to functional data analysis as described in the following
111 section.

112 **3 Functional data analysis approach**

113 **3.1 Construction of the functional data**

114 The modeling of the mean seasonal cycle of temperature uses the techniques of Functional Data Analysis (FDA), a relatively
115 novel statistical approach (Ramsay and Silverman, 2005; Horváth and Kokoszka, 2012; Kokoszka and Reimherr, 2017). Unlike
116 traditional statistics, a single observation of a variable is not a data point but rather a function. This approach is especially
117 suitable for a series of observations with an underlying correlation structure.

118 Generally, the relation between a covariate x and a response Y can be modeled as a function $y = f(x)$ using the data pairs (x_i, Y_i) with $i = 1, \dots, n$. In our case, the covariate x is represented by the days of the year (x_i varies from 1 to 365, for leap years,
119 values for February 29 were deleted). The mean seasonal cycle of temperature plays the role of response Y . To account for the
120 periodic nature of the data, the function $f(x)$ is defined as a linear combination of Fourier basis functions:

$$122 \quad f(x) = a_0 + \sum_{n=1}^m \left(a_n \cos \cos \frac{n\pi x}{365} + b_n \sin \sin \frac{n\pi x}{365} \right) \quad (1)$$

123 i.e., $f(x)$ depends on $K=2m+1$ coefficients $\{a_0, a_1, b_1, \dots, a_m, b_m\}$ and basis functions (see Fig. 1a for $K=5$).

124 The coefficients $\{a_0, a_1, b_1, \dots, a_m, b_m\}$ are chosen to minimize the following functional:

$$125 \quad \sum_{i=1}^n [Y_i - f(x_i)]^2 \quad (2)$$



126 Our approach fits a function f with varying degrees of freedom to the data. In contrast to a simple interpolation, this does not
127 necessarily mean that the function just connects all adjacent data points (i.e., in all cases where the degrees of freedom are less
128 than the number of data points, see Fig. 1). In general, the particular values, x_i , of the covariate and the corresponding observed
129 responses, Y_i , are linked by $Y_i = f(x_i) + \varepsilon_i$, $i = 1, \dots, m$, where ε_i are realizations of the random errors. This corresponds to the
130 situation where the covariate, x_i , is given, and the observed response, Y_i , is the realization of some random variable linked with
131 the value of x_i . The resulting function f balances the size of the errors, ε_i , and the smoothness of the function linking the
132 covariate and the response. The smaller the number of basis functions K is, the less sensitive it is to fluctuations in the data –
133 compare panels (b) and (d) in Fig. 1 for cases $K=5$ and $K=55$. Here we choose $K=15$. The choice is supported by the fact that
134 for this value, the character of the FDA curve best resembles the 30-day running average. The 30-day average is analogous to
135 the monthly mean, and the length of the month is an intuitive choice in climatology, as generally a lot of climatological analysis
136 is based on monthly mean values. Moreover, even for $K=5$, the FDA function explains more than 99% of the variance of the
137 30-year mean temperature values, even though the curve does not entirely align with the underlying data (Fig. 1(b)). On the
138 other hand, for higher K , the curve becomes too fluctuating, resembling high inter-daily variability in the data. Therefore, we
139 consider smoothing based on $K=15$ appropriate for the current study. However, the analysis results are not sensitive to the
140 choice of K (not shown). The FDA-smoothed curves of the mean annual cycle for all the datasets and geographical regions are
141 shown in the supplemental Fig. S03 and S07 for the historical periods, and in Fig. S04 and S08 for the projections.

142 **3.2 FDA diagnostics**

143 Drawing on the FDA representation of the annual cycle in each period specified in Table 3, we now define diagnostics that
144 evaluate changes in the shape of the annual cycle (sections 3.2.1 - 3.2.5). Fig. 2 illustrates the interpretation of the diagnostics
145 on example data. Table 4 provides an overview of the diagnostics and references to the figures showing the results based on
146 them. All the diagnostics are further used to quantify differences between the annual cycle curves in the two historical periods
147 and between the future and reference periods. For the historical periods, we compare the GCMs with ERA5 and CERA20C.
148 For future time periods, we compare individual GCMs with their multi-model mean. We want to emphasize that in the
149 projections, the multimodel mean values are based on the multimodel mean annual cycle, not the multimodel mean of the FDA
150 diagnostics. Therefore, the multimodel mean values of FDA diagnostics can fall outside the range of individual ESMs.

151 **3.2.1 Annual cycle shape**

152 For each day of the year, we calculate the distances between the smoothed annual cycle curves (see Fig. 2 (a)). We then
153 aggregate these distances in three ways: by calculating the 10th and 90th percentiles and the root mean square of them. The
154 former two diagnostics, hence, represent high and low annual extremes of the temperature changes (allowing both positive and
155 negative values), while the latter diagnostic evaluates the Euclidean distance of the whole annual cycles (positive by definition).
156 Supplemental Fig. S01 and S02 show the occurrence of values below/above 10th/90th percentiles; the red dashed line



157 represents the 10th percentile, and the green dashed line represents the 90th percentile. For all values below/above the 10th/90th
158 percentile threshold, the time periods of the year when these values occur are shown in red/green.

159 **3.2.2 Annual cycle maximum**

160 We define the shift in the annual cycle maximum as the number of days between the maximum of the annual cycle in two
161 periods (black arrow in Fig. 2(b)). Positive values indicate a delay in the maximum occurrence relative to the reference period,
162 and negative values vice versa. In regions with two (local) maxima in the annual cycle, the “first” and “second” maxima are
163 considered chronologically from January 1st, with no regard to the actual maximum magnitude (the second maximum can
164 potentially have a higher temperature than the first). There are nine regions, where we identify two distinct maxima, see Fig.
165 5, 6, S03, S04.

166 **3.2.3 Annual cycle velocity**

167 We calculate 1st derivative of the smoothed curve of the temperature annual cycle. We define temperature velocity as the
168 absolute value of this 1st derivative curve. It gives an indication of the steepness of the annual cycle on individual days (see
169 Fig. 2 (c)). Then we calculate changes in temperature velocities between corresponding days of the year between the two time
170 periods. Positive differences in temperature velocity, hence, indicate days where the annual cycle is getting steeper compared
171 to the reference period, and vice versa for negative values. Note that steepness means faster warming as well as faster cooling
172 because we consider absolute values of the 1st derivative. Similarly to the changes in temperature itself (3.2.1), we calculate
173 the 10th and 90th percentiles of the differences and their root mean square.

174 **3.2.4 Annual cycle amplitude**

175 The amplitude of the annual cycle is defined as the difference between the maximum and the minimum value in °C (see Fig.
176 2 (d)). Here we evaluate the change in the amplitude between two time periods. Consequently, a positive change in the
177 amplitude indicates an increasing temperature range over the year compared to the reference.

178 **4. Results**

179 Here, we discuss changes in the four diagnostics from a high-level perspective; detailed figures for each of the regions can be
180 found in the Supplement (see Table 4 for an overview).

181 **4.1 Changes in the shape of the annual cycle**

182 In the often employed annual-mean view, warming is evident almost everywhere on the globe, with land areas and higher
183 latitudes generally warming faster (Gulev et al., 2021). Our approach resolves seasonal differences in the long-term warming
184 signal and reveals that differences in the historical period between 1951-1980 and 1981-2010 can be negative during (short)



185 parts of the year in many regions (Fig. 3b). This is compensated by a strong warming in other parts of the year, which can
186 exceed 2 °C in many northern hemisphere land regions (Fig. 3c).

187 Fig. 3a shows the resulting aggregated differences in the shape of the seasonal cycle as the root-mean-square of the daily
188 differences (RMSD, also termed Euclidean distance), which also exceed 1.5 °C in most datasets at northern mid-latitude land
189 regions. In most other parts of the world, except Antarctica, the RMSD remains lower than 1.5 °C for the historical periods.
190 We stress that this diagnostic embraces both negative and positive temperature changes, evaluating the overall change in the
191 shape of the annual cycle, unlike simply averaging the changes over the year.

192 With regard to warming, in general, a stronger signal is seen in the northern hemisphere than in the southern hemisphere. An
193 exception is the strong warming signal in CERA20C in Antarctica (Fig. 3). Larger disagreement between the reanalyses also
194 occurs over the southern ocean and in some regions near the equator (e.g., SAH and ARP).

195 With regard to the timing, both reanalyses show the highest temperature increase during northern-hemisphere winter, or the
196 changes do not have any distinct maximum/minimum (Fig. S01). Only in New Zealand (NZ), the Southern Ocean (SOO), and
197 Antarctica (WAN and EAN) are the changes larger in the southern-hemisphere winter. In the ESMs, the timing of the largest
198 increase/decrease often does not match the reanalyses (e.g., over Greenland, the reanalyses show a decrease of temperature in
199 the first three months of the year, whereas the ESMs show the decrease (if any) later in the year, Fig. S01). In the Arctic region
200 (ARO), the ESMs and reanalyses generally agree that the lowest increase in temperature occurs in summer.

201 For the warming at the end of the 21st century, the Arctic stands out with temperature increase exceeding 10 °C in all models
202 during the 10% of strongest warming days (Fig. 4c). Such stronger warming in the polar regions compared to lower latitudes
203 (often referred to as polar amplification) is consistent with theoretical considerations and historical observations (e.g., Stuecker
204 et al., 2018; Previdi et al., 2021). Here, we show that the stronger warming at high latitudes predominantly comes from the
205 upper end of the annual temperature distribution, with the 10th percentile of changes being mostly uniform across latitudes
206 (Fig. 3b and 4b).

207 Polar amplification has also been reported to be underestimated in CMIP6 models (Casado et al., 2023) and to be weaker in
208 Antarctica than in the Arctic region in both observations and CMIP6 models (e.g., Zhang et al., 2023; Xie et al., 2022). Our
209 results contradict these results to some extent. Mainly, the five ESMs simulate the magnitude of historical warming in the
210 Arctic, higher or comparable to the reanalyses (Fig. 3). Finally, we note that in the historical period, one of the two observation-
211 based reanalyses, CERA20C, shows stronger warming in Antarctica than in the Arctic, contradicting. This discrepancy might
212 be attributable to high decadal variability in Antarctica (Casado et al., 2023) and large uncertainties of the reanalysis outputs
213 over this remote region with low density of assimilated observations (Laloyaux et al., 2018).

214 **4.2 Shift of the annual cycle maximum**

215 For the end of the 21st century, the five selected ESMs project a delayed maximum near the poles and an earlier maximum in
216 many tropical continental regions (Fig. 6). The shift of the maximum between the two historical periods does not show such
217 distinct pattern (Fig. 5). In Europe, the southern and eastern regions experienced a delay of maximum of up to 10 days,



218 whereas northern Europe a slightly earlier maximum. In North America, a similar dipole pattern is seen between eastern and
219 western regions (Fig. 5).

220 The largest differences between the reanalyses and ESMs are found over southern America and eastern and southern Africa
221 (Fig. 5). Also, in the land regions near the equator, there is a disagreement between the two reanalyses (e.g., WSAF, MDG,
222 ESAF in Africa, and NWS and SAM in South America). This is mainly due to the fact that the annual cycle has no distinct
223 maximum peak and the warm season part of the annual cycle is rather flat; thus, a small temperature change in this season may
224 result in a large shift of the maximum (Fig. S03). In North-Central America (NCA), even though it is farther from the equator,
225 CERA20C gives a large shift of the maximum, but the actual temperature change is small, similar to regions NWS and SAM
226 in South America, which are closer to the equator. In most of the regions further from the equator, the reanalyses agree on the
227 sign of the shift in the maximum. In the oceanic regions near the equator, the reanalyses show a shift to an earlier onset of the
228 maximum. Both between the two historical periods and between the reference and future period, we see a smaller shift of the
229 maximum in Antarctica than in the Arctic (Fig. 5, 6).

230 In the regions near the equator, there are two distinct maxima of the annual cycle (Fig. S03, S04); therefore, we evaluate the
231 shift also for the second maximum (Fig. 5). We stress that the first/second refers to the earlier/later occurrence during the year,
232 not to the magnitude. In some of these regions, the annual cycle has even more “maxima”; it is modulated by at least three
233 peaks (Fig. S03, e.g., CNRM-ESM2 in north-eastern Africa (NEAF)). As the amplitude of the annual cycle is generally low
234 in near-equator regions, the whole curves are rather flat, and it is difficult to compare them between the datasets. For example,
235 in the oceanic part of south-eastern Asia (SEA region), the CERA20C reanalysis shows a large shift in the 2nd maximum (Fig.
236 5). However, in Fig. S03 it is clear that in the first historical period, the annual cycle near the 2nd maximum is very flat, and
237 therefore the large shift rather indicates a clearer emergence of the 2nd maximum. Also, in north-eastern Africa (NEAF), the
238 evaluation of the maximum shift is rather problematic. The maxima in different ESMs and reanalyses are shifted, so it is
239 actually questionable to compare them (Fig. S03). Similarly, in north-west southern America (NWS), the mean annual cycle
240 in the historical periods has, according to the reanalyses, only one distinct maximum (Fig. S03). However, the ESMs show a
241 second maximum. We do not consider it in our analysis, but it is interesting to note that the annual cycle in this region is
242 projected to change in the way that the temperature at this second maximum, not present in reanalyses, becomes higher than
243 the first maximum (Fig. S04). As the annual cycle in the near-equator regions is closely related to the seasonal distribution of
244 precipitation, the shift of the maximum can indicate the change in the occurrence of dry and wet seasons. Over Africa, the first
245 maximum is projected to occur earlier, and the second maximum is expected to be delayed. We note that in above mentioned
246 regions with rather flat maximum and low amplitude, the ESMs and reanalyses mostly disagree on changes in amplitude (see
247 Section 4.4).

248 **4.3 Annual cycle velocity**

249 Higher latitudes detect a higher magnitude of temperature velocity change than lower latitudes. For future changes, the
250 geographical pattern of projected temperature velocity change remains the same as between the historical periods, with the



251 magnitude of change twice as high in most of the regions (Fig. 8). The velocity change over the oceans is mostly smaller
252 compared to the continents (Fig. 7, 8). Between the two historical periods, all regions experienced both a decrease and an
253 increase in the slope of the annual cycle, depending on the time of year (see Fig. 7 b, c and Fig. S05). Recent changes in
254 temperature velocity are largest in the western-central part of Euroasia (EEU, WSB, and ESB; Fig. 7). Generally, the regions
255 with larger changes in velocity have a larger range between the 10th and 90th percentiles, which is expected given the definition
256 of the diagnostic.

257 The temperature velocity changes agree between the reanalyses, except for Antarctica and the RFE (eastern Asia), and CNA
258 (central North America) regions. Further, the ESMs tend to underestimate the reanalysis-based velocity changes in the middle
259 and higher latitudes of the northern hemisphere, and largely agree on the smaller changes in the tropics and over the southern
260 hemisphere. The temperature velocity changes between the two historical periods are mostly in the interval between -0.1 and
261 +0.1 °C/day. This change of slope of the annual cycle curve can result in a temperature change of 3 °C per month. It naturally
262 corresponds to changes in the amplitude of the annual cycle and changes in the temperature contrasts between seasons.
263 However, Fig. S05 shows that the changes in the velocity are, in most cases, rather variable during the year, with the sign
264 persisting not for the whole season, but rather for a week up to two months. Still, except for a couple of regions, the two
265 reanalyses have rather similar annual cycle of temperature velocity changes in the historical periods. Unlike the temperature
266 change, the reanalyses agree on the sign and value of annual cycle velocity change over Greenland.

267 The five ESMs mostly follow the reanalysis-based pattern of change in temperature velocity. If there is any disagreement, the
268 models tend to underestimate the magnitude of changes. This is mainly seen in the northern hemisphere's higher latitudes.
269 Generally, over the northern hemisphere continents, we mostly see higher fluctuation of velocity changes between negative
270 and positive values in winter than in summer. Regarding the projections, Fig. S06 depicts a distinct annual cycle of velocity
271 changes in the regions where the expected warming is larger in one of the seasons. A nice example is the Arctic, where we can
272 see a decrease in velocity in the spring and the autumn, but near-zero or positive changes in winter and summer (Fig. S06).
273 This stems from a flattening of the annual cycle and higher warming in winter than in summer. In northern mid-latitude regions,
274 the velocity changes are more variable during winter than in summer (Fig. S06), which is connected to a higher increase of
275 temperature in winter than in summer and shrinking amplitude, as discussed below.

276 **4.4. Annual cycle amplitude**

277 Both reanalyses agree on the prevailing decrease in amplitude, with the largest changes detected in EEU (eastern Europe) and
278 WSB (western Siberia), CNA, NWN (both northern America), the Arctic ocean, and Antarctica (Fig. 9). Unlike the temperature
279 change, both reanalyses show that the amplitude change in the Arctic is larger than in Antarctica. The ESMs, in turn, show
280 diverging changes of amplitude between the historical periods over the globe. Over the oceans, we see small amplitude changes
281 with varying signs in both models and reanalyses, except for the Southern Ocean and the Arctic region, where all the models
282 and reanalyses show an amplitude decrease (ERA5 -0.4 and CERA20C -1.1 °C in SOO, ERA5 -2.9, CERA20C -1.6 °C).
283 Clearly, decreasing annual cycle amplitude arises from a faster increase of temperature in the colder part of the year, in



284 comparison to the warm season (Fig. S07). Such seasonal difference in temperature trends during the 20th century has been
285 reported by Nigam et al. (2017) for the northern hemisphere. However, there are several regions where the reanalyses show
286 an increase in amplitude, up to 0.8 °C, e.g., Greenland, the southern part of South America, Madagascar, and interestingly also
287 Siberia (RAR) and some regions in northern America (Fig. 9). The ESMs show decreasing amplitude everywhere. We
288 hypothesize that the discrepancy between ESMs and reanalyses over Greenland could be connected to differences in the
289 evolution of sea ice between simulations. A recent increase in amplitude over Greenland has also been reported by Deng and
290 Fu (2023).

291 In many regions, the projected future amplitude changes have the sign opposite to the changes between the historical periods
292 (compare Fig. 9 and 10). The largest increase is projected over the Mediterranean and West-Central Asia regions (due to
293 summer warming being more than winter), and the largest decrease over the Arctic Ocean (due to winter warming being higher
294 in winter than summer). Generally, the amplitude increase is projected for most of the southern hemisphere and equatorial
295 areas, whereas most of the middle to higher latitudes of the northern hemisphere are projected to experience a decrease in the
296 amplitude. There are a few exceptions: West-Central Europe (WCE), East-Central Asia (ECA), and the western part of the
297 USA (WNA), where we can see an increase in the amplitude of app. 2 - 3 °C. The increasing amplitude indicates an increase
298 in thermal continentality of climate, with higher contrasts between winter and summer.

299 To illustrate how the individual FDA diagnostics complement each other, the projected amplitude changes correspond very
300 well to the projected temperature velocity changes; a higher increase in velocity is connected to a higher decrease in amplitude,
301 and the other way around.

302 **5. Discussion**

303 The shape of the mean temperature annual cycle can be considered a very basic feature of climate. Nonetheless, we highlight
304 large observational uncertainty related to its recent changes, i.e., distinct differences between the two reanalyses, especially
305 over equatorial and polar regions. Multiple differences between the reanalyses might be behind the discrepancies. Besides
306 differences in spatial resolution, CERA20C is a coupled reanalysis, whereas ERA5 was produced by the atmospheric model
307 only. Laloyaux et al. (2018) emphasize that the former is expected to be more realistic in terms of ocean heat balance and
308 ocean heat uptake, important for the temporal evolution of near-surface air temperature and its low-frequency variability.
309 Regarding the discrepancies over Antarctica, the assimilated observations are scarce and might be spurious (Laloyaux et al.,
310 2018). Furthermore, as pointed out by, e.g., McKinon et al. (2024), the reanalysis performance is in general questionable over
311 regions that have spurious observations, not only in Antarctica but also over large portions of Africa or Southern America.
312 Furthermore, Yettella and England (2018) emphasized large internal climate variability uncertainty connected to the evolution
313 of annual cycle shape over northern hemisphere middle and high latitudes.
314 Even though we analyze only five CMIP6 ESMs, which is admittedly a very small subset of the whole multi-model ensemble,
315 they differ in many aspects, including spatial resolution (Table 2), model family (Merrifield et al., 2023), and climate sensitivity



316 (Table 2, Meehl et al., 2020). It is not thus surprising that they show diverse outcomes. They are not always able to reproduce
317 the reanalysis-based historical changes, and their projections differ in many aspects. The differences in the structure of the
318 models imply different character of internal climate variability, which is certainly behind some of the discrepancies. ESMs
319 with higher climate sensitivity generally project larger annual cycle shape changes (e.g., CanESM5 in the Arctic, Fig. 3, 4).
320 Even though it has been argued that the higher sensitivities are not plausible (e.g., IPCC, 2021), it is difficult to rule out the
321 hot models, especially in the case of regional impact assessment (Palmer et al., 2023; Swaminathan et al., 2024).
322 Previous studies on changes in the annual cycle mostly concentrated on the amplitude and shift of the maximum. Chen et al.
323 (2019) studied ERA-Interim-based and CMIP5-simulated spatial patterns of seasonal amplitude and phase. They concluded
324 that the seasonal amplitude reduced during the 21st century over high latitudes of both hemispheres because cold-season air
325 temperature increases faster than warm-season air temperature. In contrast, over low latitudes, the expected evolution is exactly
326 the reverse. Further, the maximum of the annual cycle was projected to be delayed by 15 - 30 days over the high-latitude
327 oceans where the sea ice is expected to shrink significantly (Chen et al., 2019). All these patterns are also obvious in our
328 results, implying consistency between CMIP5 and CMIP6 projections. The gradual decrease of amplitude prevailing over most
329 of the northern hemisphere has also been reported in other studies, including Stine and Huybers (2012), Wang and Dillon
330 (2014), Nigam et al. (2017), and Cornes et al. (2018). However, we depict some regions where the reanalyses disagree on the
331 sign of change, and also regions where both ESMs and reanalyses imply an increase in the amplitude. Delayed onset of annual
332 cycle maximum over most of the northern-hemisphere continents was also reported by Deng and Fu (2023).
333 In a recent study, Brunner and Voigt (2024) revealed a systematic bias in the definition of percentile-based temperature
334 extremes (Tx90p) when using too long seasonally running windows. One of the pitfalls they revealed was spurious signals of
335 change in Tx90p, as the strength of the bias depends on the shape of the temperature annual cycle (as well as the day-to-day
336 variability). They find two particularly affected regions: a region of increasing bias in oceans north of 45°N, except the very
337 highest latitudes (approximately our NPO, NAO, and MED regions), and a region of decreasing bias in our ARS region (see
338 their Fig. 5a). Connecting to our results, stronger seasonal gradients (corresponding to a higher temperature velocity) favour a
339 stronger bias in Tx90p (Brunner and Voigt 2024). Indeed, we find a weak (in particular compared to some land regions; see
340 Fig. 8), but clear increase in temperature velocity between 1961-1990 and 2071-2100 in all three regions affected by increasing
341 bias (NPO, NAO, MED), which is particularly pronounced towards and away from the annual maximum (which is located
342 around end of August/beginning of September or day of the year 240, Fig. S04). While the absolute value of the temperature
343 velocity change is considerably higher in other regions, its systematic increase in combination with the low day-to-day
344 temperature variability considerably contributes to the increase in Tx90p bias in these regions.
345 For the region of decreasing bias in Brunner and Voigt (2024), roughly corresponding to our ARS region, the attribution of
346 the bias change to the temperature velocity is less clear due to a combination of two reasons; first, the decreased bias stems
347 mainly from a very limited number of days surrounding the second annual minimum in the region (July and September; see
348 Fig. 5c in Brunner and Voigt 2024). For CanESM5, which was used in Brunner and Voigt (2024), we do find a short consistent
349 decrease in the temperature velocity corresponding to those months (Fig. S06). Second, the decrease in bias found in this



350 region is also (at least partly) attributable to an increase in day-to-day variability, which is not evaluated by the FDA
351 diagnostics.

352 **Conclusions**

353 This paper presented an innovative method for assessing the shape of the annual cycle. It is applicable for different climatic
354 variables and for various purposes, with no need to make any prior assumptions about the annual cycle shape. The diagnostics
355 we introduced provide important information about different aspects of the seasonal cycle shape and its changes: amplitude,
356 slope, and location of extrema. We analyze annual cycles averaged over 30-year periods. However, the method can also serve
357 to analyze shorter-term variability of the seasonal cycle and even study inter-annual variability of the shape features. Unlike
358 methods based on monthly or seasonal means (e.g., evaluating the amplitude based on monthly values), the FDA diagnostics
359 can capture even slight changes in the shape of the annual cycle, for example, in the timing of the maximum, discussed in
360 Section 4.2.

361 We have illustrated the methodology by using the example of the annual temperature cycle and its changes in pre-defined
362 climatological regions. We used it to assess recent and projected changes in the annual temperature cycle in a selection of
363 ESMs and observation-based datasets. Other potential applications include assessing other variables or evaluating the model
364 performance explicitly. Differences between models and one or more reference datasets would be investigated in the latter
365 case. The results can be aggregated, assessing the ensemble mean and spread. The diagnostics can be modified to evaluate not
366 only changes between time periods, but also differences between datasets to reveal model biases in the representation of the
367 annual cycle compared to an observational reference. The definition of FDA diagnostics can thus be tailored for specific
368 interests and applications.

369

370 **Supplement:**

371 Additional figures S01-S08.

372 **Interactive computing environment**

373 Jupyter notebooks are published in Zenodo: DOI: 10.5281/zenodo.15866118

374 **Code availability**

375 Jupyter notebooks are published in Zenodo: DOI: 10.5281/zenodo.15866118



376 **Data availability**

377 Underlying CMIP6 data were downloaded from the ETH Zurich CMIP6 next generation archive (Brunner et al., 2020), but
378 are also freely available in the ESGF. The underlying ERA5 data are freely available from the Copernicus Climate Data Store.
379 Data from CERA20C reanalysis were downloaded from ECMWF with the help of Jan Masek from the Czech
380 Hydrometeorological Institute. Preprocessed data used for the FDA calculations are published in Zenodo: DOI:
381 10.5281/zenodo.15866118. For any details or requests, please contact one the corresponding authors.

382 **Author contribution**

383 EH: Conceptualization, data pre-processing, interpretation of the results, writing of the draft. LB: Conceptualization, data pre-
384 processing, plotting, interpretation of the results. JK: Methodology development, FDA calculations, coding, and plotting. All
385 three authors have contributed to the writing of the final text.

386 **Competing interests**

387 The authors declare no competing interests.

388 **Acknowledgements**

389 We acknowledge the CMIP community for providing the climate model data, retained and globally distributed in the
390 framework of the ESGF.

391 We acknowledge the European Centre for Medium-Range Weather Forecasts (ECMWF) for producing the ERA5 (Hersbach
392 et al., 2020) and CERA20C (Laloyaux et al., 2018) reanalyses.

393 We acknowledge the World Climate Research Programme's Working Group on Coupled Modelling, which is responsible for
394 CMIP, and we thank the climate modeling groups for producing and making available their model outputs.

395 For CMIP, the US Department of Energy's Program for Climate Model Diagnosis and Intercomparison provides coordinating
396 support and led the development of software infrastructure in partnership with the Global Organization for Earth System
397 Science Portals.

398 We thank the Copernicus Climate Change Service, ECMWF, and the ETH Zurich CMIP6 next generation archive (Brunner et
399 al., 2020).

400 Data from CERA20C reanalysis were downloaded from ECMWF with the help of Jan Masek from the Czech
401 Hydrometeorological Institute.



402 **Financial support**

403 This research was partly supported by the program of the Charles University Cooperatio "Sci-Physics". LB has received
404 funding by the Deutsche Forschungsgemeinschaft (DFG, German Research Foundation) under Germany's Excellence Strategy
405 EXC 2037 'CLICCS—Climate, Climatic Change, and Society' - Project No. 390683824, a contribution to the Center for Earth
406 System Research and Sustainability (CEN) of the University of Hamburg. EH and JK were supported by the grant GA25-
407 15855S of the Czech Science Foundation.

408 **References**

409 Abramowitz, G., Herger, N., Gutmann, E., Hammerling, D., Knutti, R., Leduc, M., Lorenz, R., Pincus, R., and Schmidt, G.
410 A.: Model dependence in multi-model climate ensembles: Weighting, sub-selection and out-of-sample testing, *Earth Syst.
411 Dynam.*, 10, 91–105, doi:10.5194/esd-10-91-2019, 2019.

412 Bordoni, S., Kang, S. M., Shaw, T. A., Simpson, I. R., and Zanna, L.: The futures of climate modeling, *NPJ Clim. Atmos. Sci.*,
413 8, 1, doi:10.1038/s41612-025-00955-8, 2025.

414 Bock, L., Lauer, A., Schlund, M., Barreiro, M., Bellouin, N., Jones, C., et al.: Quantifying progress across different CMIP
415 phases with the ESMValTool, *J. Geophys. Res. Atmos.*, 125, e2019JD032321, doi:10.1029/2019JD032321, 2020.

416 Brunner, L., Hauser, M., Lorenz, R., and Beyerle, U.: The ETH Zurich CMIP6 next generation archive: technical
417 documentation, *Zenodo*, doi:10.5281/zenodo.3734128, 2020.

418 Brunner, L. and Voigt, A.: Pitfalls in diagnosing temperature extremes, *Nat. Commun.*, 15, 2087, doi:10.1038/s41467-024-
419 46349-x, 2024.

420 Casado, M., Hébert, R., Faranda, D., & Landais, A.: The quandary of detecting the signature of climate change in Antarctica,
421 *Nat. Clim. Change*, 13(10), 1082–1088, doi:10.1038/s41558-023-01791-5, 2023.

422 Chen, J., Dai, A., & Zhang, Y.: Projected changes in daily variability and seasonal cycle of near-surface air temperature over
423 the globe during the twenty-first century. *Journal of Climate*, 32(24), 8537–8561, doi:10.1175/JCLI-D-19-0438.1, 2019.

424 Cornes, R. C., Jones, P. D., & Qian, C.: Twentieth-century trends in the annual cycle of temperature across the Northern
425 Hemisphere, *J. Clim.*, 30(15), 5755–5773, doi:10.1175/JCLI-D-16-0315.1, 2017.

426 Deng, Q., and Fu, Z.: Regional changes of surface air temperature annual cycle in the Northern Hemisphere land areas, *Int. J.
427 Climatol.*, 43(5), 2238–2249, doi:10.1002/joc.7972, 2023.

428 Dwyer, J. G., Biasutti, M., and Sobel, A. H.: Projected changes in the seasonal cycle of surface temperature, *J. Climate*, 25,
429 6359–6374, doi:10.1175/JCLI-D-11-00741.1, 2012.

430 Eyring, V., Bony, S., Meehl, G. A., Senior, C. A., Stevens, B., Stouffer, R. J., Taylor, K. E.: Overview of the Coupled Model
431 Intercomparison Project Phase 6 (CMIP6) experimental design and organization. *Geoscientific Model Development*, 9(5),
432 1937–1958, doi:10.5194/gmd-9-1937-2016, 2016.



433 Gulev, S. K., Thorne, P. W., Ahn, J., Dentener, F. J., Domingues, C. M., Gerland, S., et al.: Changing State of the Climate
434 System, in *Clim. Change 2021: Phys. Sci. Basis*, Cambridge Univ. Press, pp. 287–422, doi:10.1017/9781009157896.004,
435 2021.

436 Hersbach, H., Bell, B., Berrisford, P., et al.: The ERA5 global reanalysis, *Q. J. R. Meteorol. Soc.*, 146, 1999–2049,
437 doi:10.1002/qj.3803, 2020.

438 Holtanová, E., Mendlik, T., Koláček, J., Horová, I., and Mikšovský, J.: Similarities within a multi-model ensemble: Functional
439 data analysis framework, *Geosci. Model Dev.*, 12, 735–752, doi:10.5194/gmd-12-735-2019, 2019.

440 Horváth, L., and Kokoszka, P.: *Inference for functional data with applications*, Vol. 200, Springer Sci. Bus. Media, 2012.

441 **IPCC: Summary for Policymakers**, in *Clim. Change 2021: Phys. Sci. Basis, Cambridge Univ.*
442 *Press*, pp. 3–32, doi:10.1017/9781009157896.001, 2021.

443 Iturbide, M., Gutiérrez, J. M., Alves, L. M., Bedia, J., Cerezo-Mota, R., Cimadevilla, E., et al.: An update of IPCC climate
444 reference regions for subcontinental analysis of climate model data: definition and aggregated datasets, *Earth Syst. Sci. Data*,
445 12(4), 2959–2970, doi:10.5194/essd-12-2959-2020, 2020.

446 Kokoszka, P., and Reimherr, M.: *Introduction to functional data analysis*, Chapman Hall/CRC, 2017.

447 Laloyaux, P., de Boisseson, E., Balmaseda, M., Bidlot, J.-R., Broennimann, S., Buizza, R., et al.: CERA-20C: A coupled
448 reanalysis of the twentieth century, *J. Adv. Model. Earth Syst.*, 10, 1172–1195, doi:10.1029/2018MS001273, 2018.

449 López-Franca, N., Sanchez, E., Menéndez, C., Carril, A. F., Zaninelli, P. G., and Flombaum, P.: Characterization of seasons
450 over the extratropics based on the annual daily mean temperature cycle, *Int. J. Climatol.*, 42(11), 5570–5585, 2022.

451 Lynch, C., Seth, A., & Thibeault, J.: Recent and projected annual cycles of temperature and precipitation in the Northeast
452 United States from CMIP5. *Journal of Climate*, 29(1), 347–365, doi:10.1175/JCLI-D-14-00781.1, 2016.

453 Marvel, K., Cook, B. I., Bonfils, C., Smerdon, J. E., Williams, A. P., and Liu, H.: Projected changes to hydroclimate seasonality
454 in the continental United States, *Earth's Future*, 9, e2021EF002019, doi:10.1029/2021EF002019, 2021.

455 McDonnell, A., Bauer, A. M., and Proistosescu, C.: To What Extent Does Discounting ‘Hot’ Climate Models Improve the
456 Predictive Skill of Climate Model Ensembles?, *Earth's Future*, 12(10), e2024EF004844, 2024.

457 McKinnon, K. A., and Huybers, P.: Inferring Northern Hemisphere continental warming patterns from the amplitude and phase
458 of the seasonal cycle in surface temperature, *J. Clim.*, 37(2), 475–485, doi:10.1175/JCLI-D-22-0773.1, 2024.

459 McKinnon, K. A., Simpson, I. R., and Williams, A. P.: The pace of change of summertime temperature extremes, *Proc. Natl.*
460 *Acad. Sci. U.S.A.*, 121(42), e2406143121, doi:10.1073/pnas, 2024.

461 Meehl, G. A., Senior, C. A., Eyring, V., Flato, G., Lamarque, J. F., Stouffer, R. J., Taylor, K. E., and Schlund, M.: Context for
462 interpreting equilibrium climate sensitivity and transient climate response from the CMIP6 Earth system models, *Science*
463 *Advances*, 6, eaba1981, doi:10.1126/sciadv.aba1981, 2020.



464 Merrifield, A. L., Brunner, L., Lorenz, R., Humphrey, V., and Knutti, R.: Climate model Selection by Independence,
465 Performance, and Spread (ClimSIPS v1.0.1) for regional applications, *Geosci. Model Dev.*, 16(16), 4715–4747,
466 doi:10.5194/gmd-16-4715-2023, 2023.

467 Nigam, S., Thomas, N. P., Ruiz-Barradas, A., and Weaver, S. J.: Striking seasonality in the secular warming of the northern
468 continents: Structure and mechanisms, *J. Clim.*, 30(16), 6521–6541, doi:10.1175/JCLI-D-16-0757.1, 2017.

469 Palmer, T. E., McSweeney, C. F., Booth, B. B. B., Priestley, M. D. K., Davini, P., Brunner, L., Borchert, L., and Menary, M.
470 B.: Performance-based sub-selection of CMIP6 models for impact assessments in Europe, *Earth Syst. Dyn.*, 14(2), 457–483,
471 doi:10.5194/esd-14-457-2023, 2023.

472 Paluš, M., Novotná, D., and Tichavský, P.: Shifts of seasons at the European mid-latitudes: Natural fluctuations correlated
473 with the North Atlantic Oscillation, *Geophys. Res. Lett.*, 32, L12703, doi:10.1029/2005GL022838, 2005.

474 Park, B. J., Kim, Y. H., Min, S. K., and Lim, E. P.: Anthropogenic and natural contributions to the lengthening of the summer
475 season in the Northern Hemisphere, *J. Clim.*, 31(17), 6803–6819, doi:doi:10.1175/JCLI-D-17-0643.1, 2018.

476 Previdi, M., Smith, K. L., and Polvani, L. M.: Arctic amplification of climate change: A review of underlying mechanisms,
477 *Environ. Res. Lett.*, 16(9), doi:10.1088/1748-9326/ac1c29, 2021.

478 Rahimpour Asenjan, M., Brissette, F., Martel, J. L., and Arsenault, R.: Understanding the influence of “hot” models in climate
479 impact studies: a hydrological perspective, *Hydrol. Earth Syst. Sci.*, 27(23), 4355–4367, doi:10.5194/hess-27-4355-2023,
480 2023.

481 Ramsay, J. O., and Silverman, B. W.: Functional data analysis, second ed., Springer, New York, 2005.

482 Randall, D. A., Bitz, C. M., Danabasoglu, G., Denning, A. S., Gent, P. R., Gettelman, A., Griffies, S. M., Lynch, P., Morrison,
483 H., Pincus, R., and Thuburn, J.: 100 Years of Earth System Model Development, *Meteorol. Monogr.*, 59, 12.1–12.66,
484 doi:10.1175/amsmonographs-d-18-0018.1, 2019.

485 Santer, B. D., Po-Chedley, S., Feldl, N., Fyfe, J. C., Fu, Q., Solomon, S. et al.: Robust anthropogenic signal identified in the
486 seasonal cycle of tropospheric temperature. *Journal of Climate*, 35(18), 6075–6100, doi:10.1175/JCLI-D-21-0766.1, 2022.

487 Santer, B. D., Po-Chedley, S., Zelinka, M. D., Cvijanovic, I., Bonfils, C., Durack, P. J., Fu, Q., Kiehl, J., Mears, C., Painter,
488 J., Pallotta, G., Solomon, S., Wentz, F. J., & Zou, C. Z.: Human influence on the seasonal cycle of tropospheric temperature.
489 *Science*, 361(6399). doi:10.1126/science.aas8806, 2018.

490 Shaw, T. A. and Stevens, B.: The other climate crisis, *Nature*, 639, 877–887, doi:10.1038/s41586-025-08680-1, 2025.

491 Snyder, A., Prime, N., Tebaldi, C., and Dorheim, K.: Uncertainty-informed selection of CMIP6 Earth system model subsets
492 for use in multisectoral and impact models, *Earth Syst. Dyn.*, 15(5), 1301–1318, doi:10.5194/esd-15-1301-2024, 2024.

493 Stine, A. R. and Huybers, P.: Changes in the seasonal cycle of temperature and atmospheric circulation, *J. Climate*, 25, 7362–
494 7380, doi:10.1175/JCLI-D-11-00470.1, 2012.

495 Stine, A. R., Huybers, P., and Fung, I. Y.: Changes in the phase of the annual cycle of surface temperature, *Nature*, 457, 435–
496 440, doi:10.1038/nature07675, 2009.



497 Stuecker, M. F., Bitz, C. M., Armour, K. C., Proistosescu, C., Kang, S. M., Xie, S. P., Kim, D., McGregor, S., Zhang, W.,
498 Zhao, S., Cai, W., Dong, Y., and Jin, F. F.: Polar amplification dominated by local forcing and feedbacks, *Nat. Clim. Change*,
499 8(12), 1076–1081, doi:10.1038/s41558-018-0339-y, 2018.

500 Swaminathan, R., Schewe, J., Walton, J., Zimmermann, K., Jones, C., Betts, R. A., Burton, C., Jones, C. D., Mengel, M.,
501 Reyer, C. P. O., Turner, A. G., and Weigel, K.: Regional Impacts Poorly Constrained by Climate Sensitivity, *Earth's Future*,
502 12(12), doi:10.1029/2024EF004901, 2024.

503 Tebaldi, C., Debeire, K., Eyring, V., Fischer, E., Fyfe, J., Friedlingstein, P., Knutti, R., Lowe, J., and others: Climate model
504 projections from the Scenario Model Intercomparison Project (ScenarioMIP) of CMIP6, *Earth Syst. Dynam.*, 12, 253–293,
505 doi:10.5194/esd-12-253-2021, 2021.

506 Wang, G., and Dillon, M. E.: Recent geographic convergence in diurnal and annual temperature cycling flattens global thermal
507 profiles, *Nat. Clim. Change*, 4(11), 988–992, doi:10.1038/nclimate2339, 2014.

508 Wang, J., Guan, Y., Wu, L., Guan, X., Cai, W., Huang, J., Dong, W., and Zhang, B.: Changing Lengths of the Four Seasons
509 by Global Warming, *Geophys. Res. Lett.*, 48(6), doi:10.1029/2020GL091753, 2021.

510 Xie, A., Zhu, J., Kang, S., Qin, X., Xu, B., and Wang, Y.: Polar amplification comparison among Earth's three poles under
511 different socioeconomic scenarios from CMIP6 surface air temperature, *Sci. Rep.*, 12(1), doi:10.1038/s41598-022-21060-3,
512 2022.

513 Yettella, V., and England, M. R.: The Role of Internal Variability in Twenty-First-Century Projections of the Seasonal Cycle
514 of Northern Hemisphere Surface Temperature, *J. Geophys. Res. Atmos.*, 123(23), 13149–13167, doi:10.1029/2018JD029066,
515 2018.

516 Zhang, Y., Kong, Y., Yang, S., and Hu, X.: Asymmetric Arctic and Antarctic Warming and Its Intermodel Spread in CMIP6,
517 *J. Clim.*, 36(23), 8299–8310, doi:10.1175/JCLI-D-23-0118.1, 2023.

518 Zhang, C., Wu, G., and Zhao, R.: Changes in the annual cycle of surface air temperature over China in the 21st century
519 simulated by CMIP6 models, *Sci. Rep.*, 15, 13661, doi:10.1038/s41598-025-18332-1, 2025.

520 Zhao, R., Wang, K., Wu, G., and Zhou, C.: Temperature annual cycle variations and responses to surface solar radiation in
521 China between 1960 and 2016, *Int. J. Climatol.*, 41, E2959–E2978, doi:10.1002/joc.7460, 2021.

522

523

524

525

526



527 **Table 1:** Basic information about the two reanalysis datasets used in the present study.

Acronym	Modeling center	Horizontal resolution of the atmospheric component (lat x lon)	Model components
ERA5	European Centre for Medium-Range Weather Forecasts (ECMWF)	0.28° x 0.28° (31 km x 31 km)	Atmosphere
CERA20 C	European Centre for Medium-Range Weather Forecasts (ECMWF)	1.125° x 1.125°	Atmosphere, Land, Ocean, Waves, Sea ice

528

529

530

531

532

533

534

535

536

537

538

539

540

541

542

543

544

545

546

547

548

549

550



551 **Table 2:** Basic information on the CMIP6 ESMs used in the present study. The values of the equilibrium climate sensitivity are taken from
552 Meehl et al. (2020).

ESM Acronym	Modelling center	Horizontal resolution (lat x lon)	Equilibrium climate sensitivity
CanESM5	Canadian Centre for Climate Modelling and Analysis, Environment and Climate Change Canada, Victoria, Canada	2.8° x 2.8°	5.6 °C
CNRM-ESM2-1	Centre National de Recherches Meteorologiques (CNRM) and Centre Europeen de Recherche et de Formation Avancee en Calcul Scientifique (CERFACS), Toulouse, France	1.4° x 1.4°	4.8 °C
EC-Earth3	EC-Earth consortium, Rossby Center, Swedish Meteorological and Hydrological Institute/SMHI, Norrkoping, Sweden	0.7° x 0.7°	4.3 °C
MPI-ESM1-2-HR	Max Planck Institute for Meteorology, Germany	0.94° x 0.94°	3.0 °C
NorESM2-MM	NorESM Climate modeling Consortium, Oslo, Norway	1.25° x 0.9°	2.5 °C

553

554

555

556

557

558

559

560

561

562

563

564

565

566



567 **Table 3:** Overview of time periods investigated in the present study.

Time period	Notation	Datasets analyzed
1951-1980	Historical (first)	Reanalyses and the five selected ESMs
1981-2010	Historical (second)	Reanalyses and the five selected ESMs
1961-1990	Reference	Five selected ESMs and their multi-model mean
2071-2100	Future/scenario	Five selected ESMs and their multi-model mean

568

569

570

571

572

573

574

575

576

577

578

579

580

581

582

583

584

585

586

587

588

589

590

591

592



593 **Table 4:** Overview of the FDA diagnostics and the corresponding figures showing the results. The “Regional figures” in the Supplement
594 show the FDA results underlying the individual diagnostics.

Diagnostic	Global figures (historical / projections)	Regional figures (historical / projections)
Annual cycle shape	Fig. 3 / Fig. 4	Fig. S01 / Fig. S02
Annual cycle maximum	Fig. 5 / Fig. 6	Fig. S03 / Fig. S04
Annual cycle velocity	Fig. 7 / Fig. 8	Fig. S05 / Fig. S06
Annual cycle amplitude	Fig. 9 / Fig. 10	Fig. S07 / Fig. S08

595

596

597

598

599

600

601

602

603

604

605

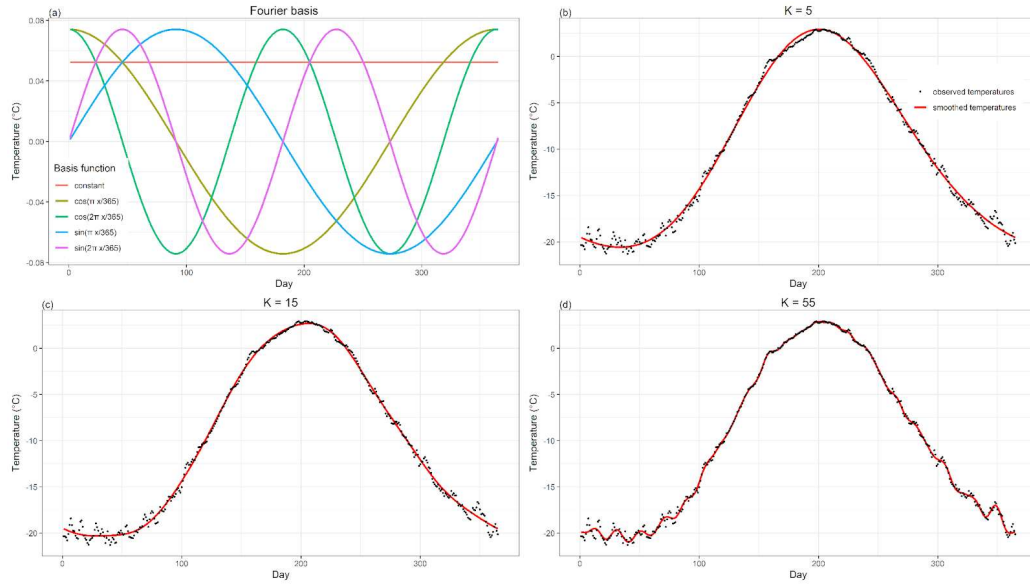
606

607

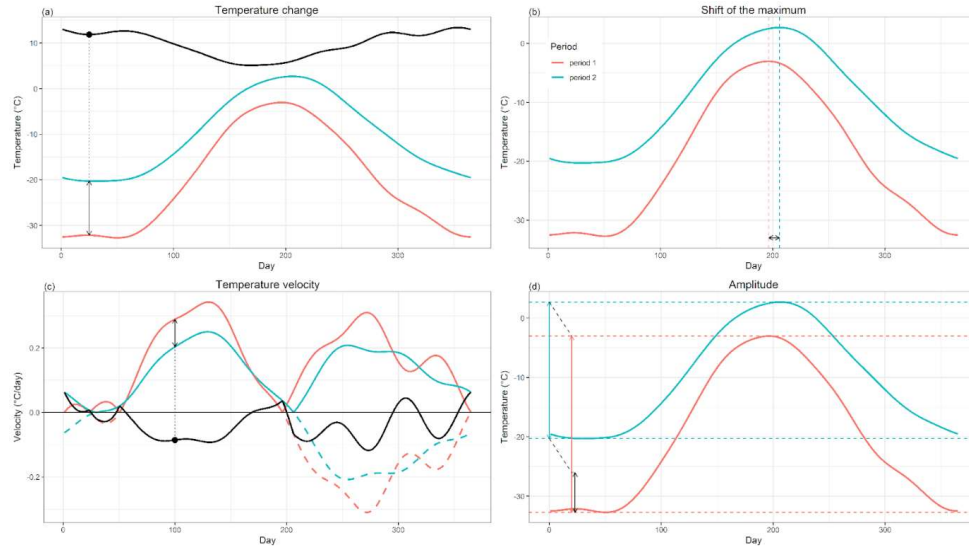
608

609

610



611
612 **Figure 1.** (a) Basis functions for the case $K=5$; (b, c, d) smoothed temperature with respect to $K = 5, 15, 55$. As the number of coefficients
613 grows more and more variability beyond the mean seasonal cycle is captured by the FDA.
614
615
616
617



618

619 **Figure 2.** The FDA diagnostics interpretation framework. Blue and red lines illustrate an example FDA-smoothed temperature annual cycle
620 in two time periods, except for panel (c), where the lines represent the absolute values of the 1st derivative of the FDA-smoothed curves,
621 i.e., temperature velocity, and the dashed color lines are used to depict negative temperature velocities. (a) The black arrow corresponds to
622 the vertical temperature change between the two periods on a specific day of the year, and the black line represents its values during the
623 whole year. (b) Dashed lines represent the days of temperature maxima, and the black arrow corresponds to the shift of the maximum. (c)
624 The black arrow corresponds to the change of temperature velocity between the two periods on a specific day, and the black line represents
625 its values during the whole year. (d) The blue and red arrows correspond to the amplitudes in each period, and the vertical black arrow
626 illustrates the change in the amplitude between the two periods.

627

628

629

630

631

632

633

634

635

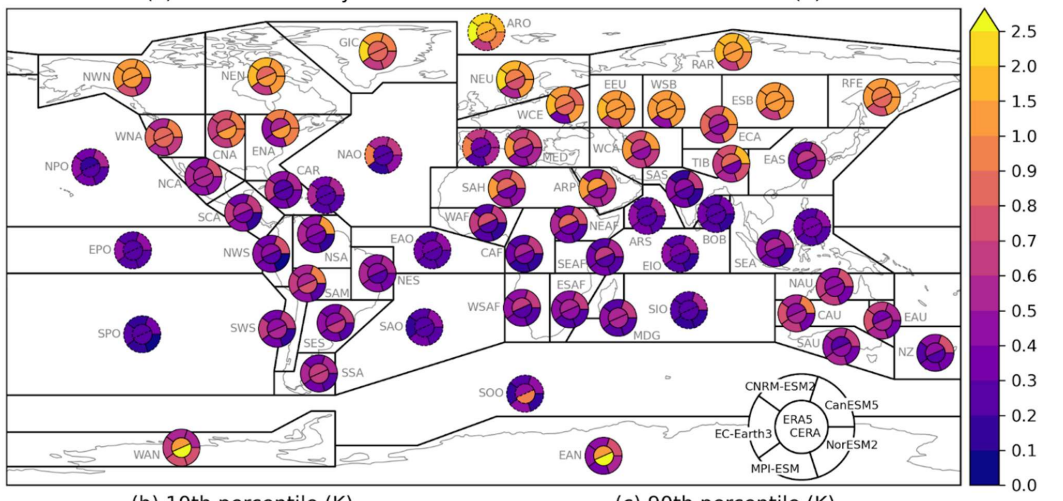
636

637

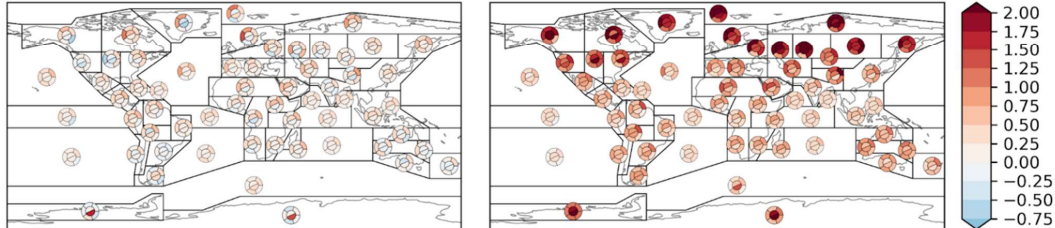


638

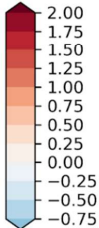
(a) RMS of annual cycle difference 1981-2010 minus 1951-1980 (K)



(b) 10th percentile (K)



(c) 90th percentile (K)



639

640

Figure 3: (a) Root mean square difference (Euclidean distance, [K]) of the whole FDA-smoothed mean annual cycle curves between the two historical periods 1981-2010 and 1951-1980. (b) 10th percentile and (c) 90th percentile of daily distances [K] between the smoothed annual cycle curves. For each region, the center of the pie plot shows results based on the two reanalysis datasets ERA5 and CERA, while the outer part of the pie shows the results for the five CMIP6 ESMs (see Section 2 for data description).

641

642

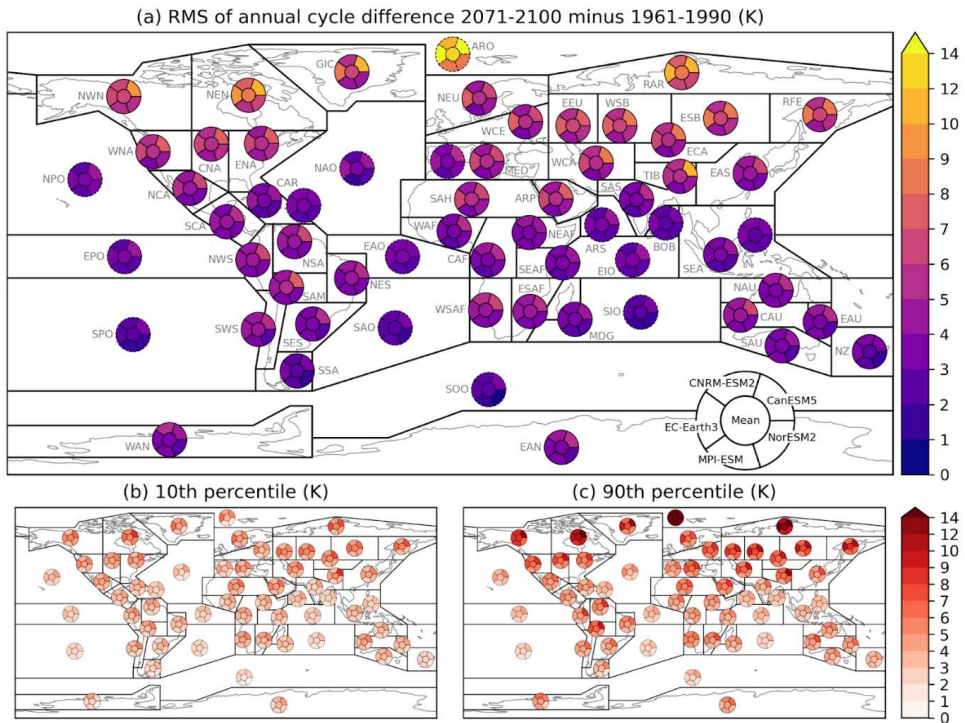
643

644

645



646



647

Figure 4: Same as Fig. 3, but for the differences between the scenario period 2071-2100 and the reference period 1961-1990. Future model simulations follow the SSP3-7.0 socio-economic pathway.

648

649

650

651

652



653

654

655

656

657

658

659

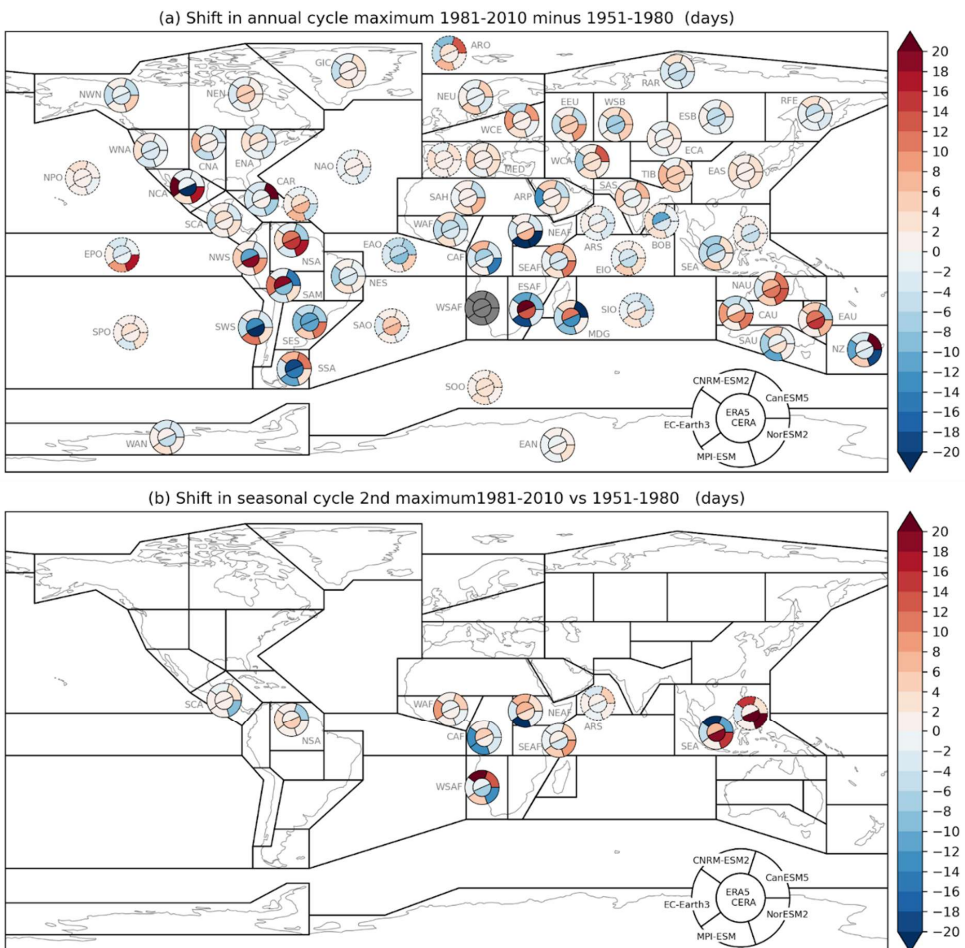
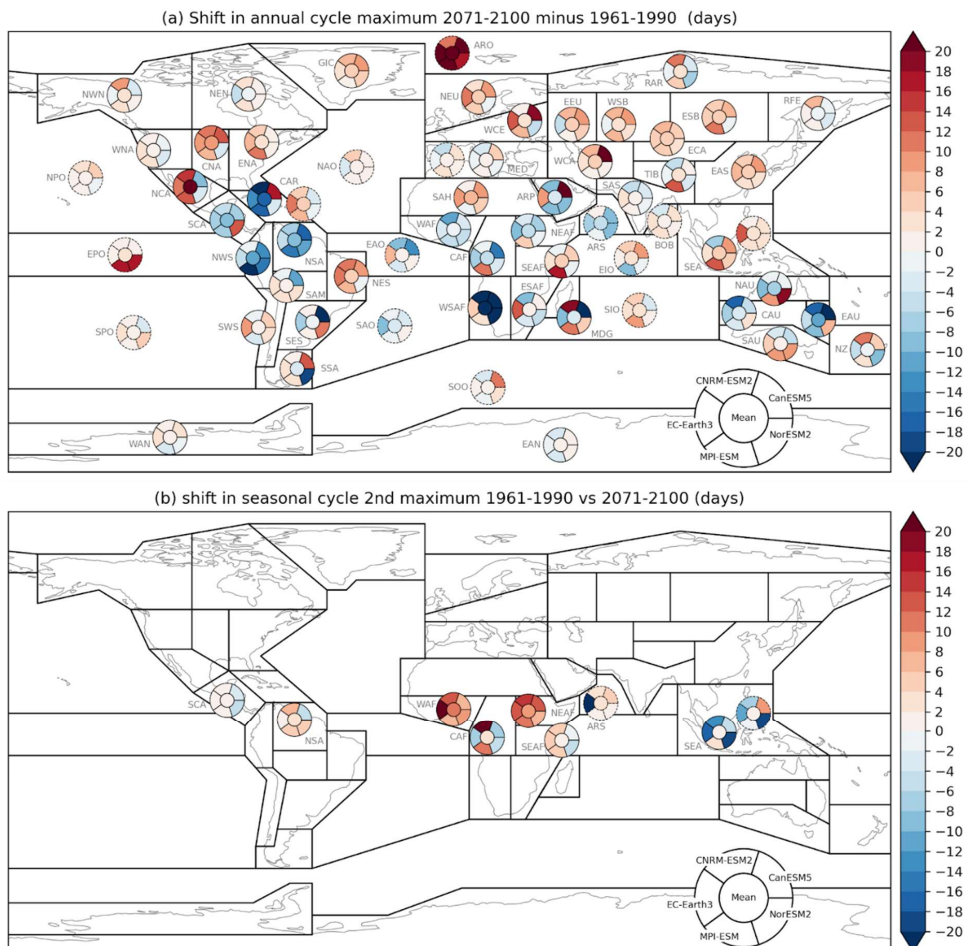


Figure 5: Similar to Fig. 3a, but for (a) shift in the annual cycle maximum and (b) shift of the second maximum in regions with two distinct maxima. Note that the “first” and “second” maxima are considered chronologically from January 1st, with no regard to the actual maximum magnitude (the second maximum can potentially have a higher temperature than the first).



660

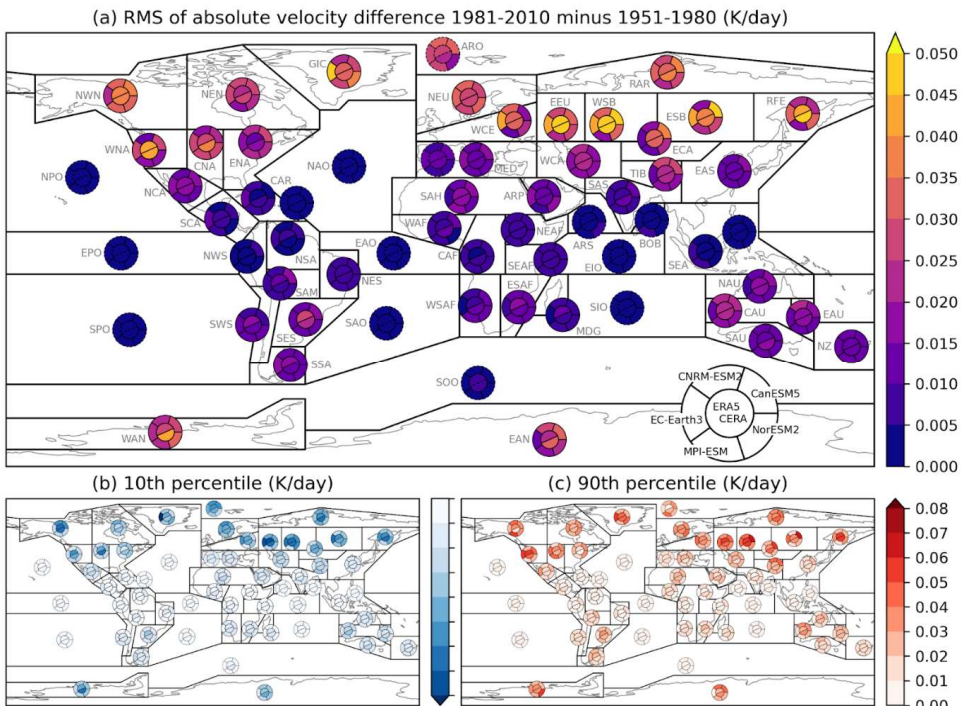


661
662

Figure 6: Same as Fig. 5, but for the shifts of the maxima between the scenario and historical periods.

663
664

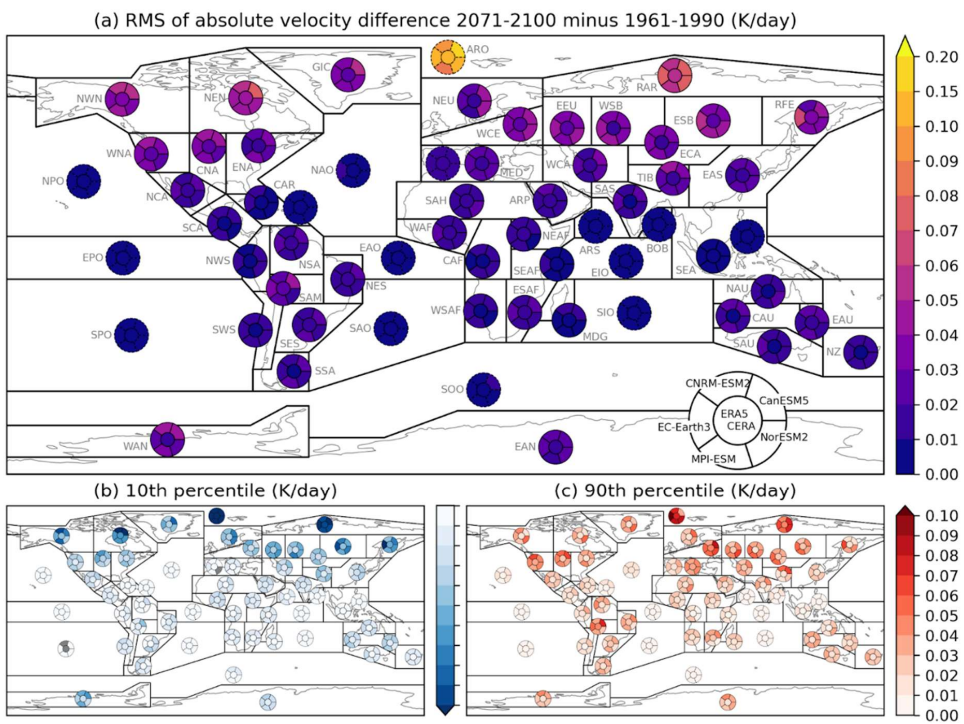
665



666

667

668 **Figure 7:** Same as Fig. 3, but for temperature velocity, that is the 1st derivative of the smoothed curve of the temperature annual cycle. Note
669 that the color scale for plot in (b) has the same range as plot (c), just reversed, i.e., negative values going from 0 K/day (white color) to -0.08
670 K/day (darkest blue). The range is not shown for the sake of better visibility of the plots.

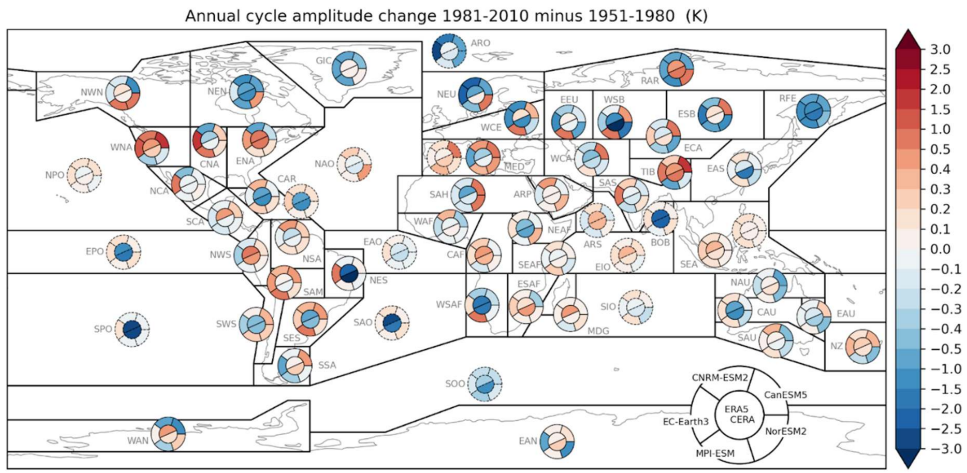


671
672

Figure 8: Same as Fig. 7, but for the change in temperature velocity between the scenario and reference periods.

673
674
675
676

677



678
679

Figure 9: Same as Fig. 3a, but for the change in the amplitude of the annual cycle.

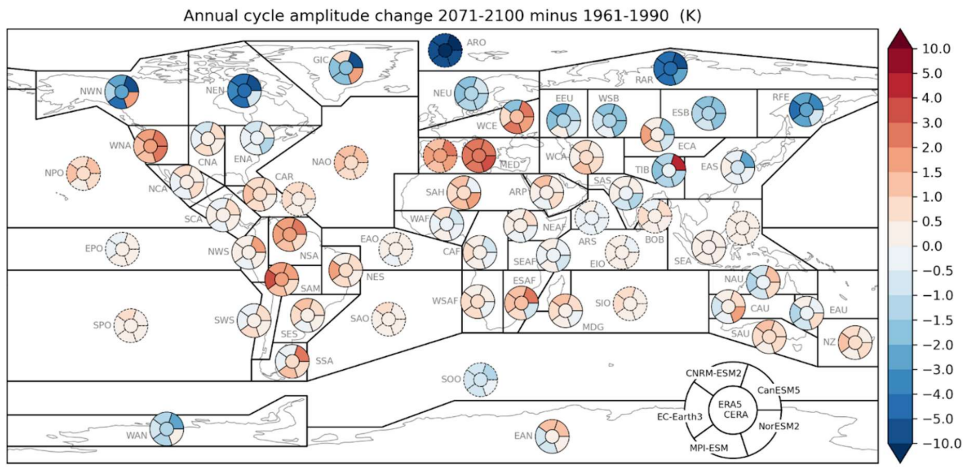
680

681

682

683

684
685



686
687

Figure 10: Same as Fig. 4a, but for the change in the amplitude of the annual cycle.

688

689

690

691